Catalysis Today 171 (2011) 84–96

Contents lists available at ScienceDirect

Catalysis Today

journal homepage: www.elsevier.com/locate/cattod

Catalytic partial oxidation of CH_4 with nickel–lanthanum-based catalysts

L.D. Vella[a], J.A. Villoria[b], S. Specchia[a,*], N. Mota[b], J.L.G. Fierro[b], V. Specchia[a]

[a] Department of Materials Science and Chemical Engineering, Politecnico di Torino – Corso Duca degli Abruzzi 24, 10129 Torino, Italy
[b] Instituto de Catàlisis y Petroleoquìmica (CSIC), C/Marie Curie 2, Cantoblanco 28049, Madrid, Spain

ARTICLE INFO

Article history:
Received 29 October 2010
Received in revised form 8 March 2011
Accepted 29 March 2011
Available online 2 June 2011

Keywords:
Syngas
Methane catalytic partial oxidation
Short contact time
Fixed bed reactor
Nickel–lanthanum catalysts
Alumina carrier

ABSTRACT

The aim of this work, concerning with the partial oxidation of methane to syngas in a self-sustained short contact time reactor using pure oxygen as oxidant, was the development of perovskite-based nickel–lanthanum ($LaNiO_3$ with Ni partially substituted by Co and Pt) catalysts and the comparison of their performance with that of 5% nickel on alumina catalyst. The prepared catalytic materials were arranged in a fixed bed and the activity tests were carried out by increasing the WHSV from ~130 to ~560 N l h^{-1} g_{cat}^{-1}. Perovskite-based catalysts were characterized by performances lower than that of 5% Ni/Al_2O_3. The very low perovskites catalytic performance towards the partial oxidation of methane was mainly due to the high reducibility of their structures into La_2O_3, metallic Ni, and Ni oxides; moreover, La and Ni species further reacted with the CPO reaction products CO_2 and H_2O leading thus to the formation of the poorly active species $La(OH)_3$, La_2NiO_4 and $La_2O_2CO_3$.

On the contrary, 5% Ni/Al_2O_3 catalyst showed a very satisfactory CH_4 conversion always above 85%, remaining stable by varying WHSV. The same trend was noticed for H_2 and CO selectivity, both around 90%. Furthermore, as concerns the bed temperature by increasing WHSV, 5% Ni/Al_2O_3 catalyst presented quite stable T_{in} and T_{out} (the latter around 1200–1250 °C), whereas the perovskite-based catalysts showed a quick T_{in} decrease and T_{out} increase, anyway not exceeding 1200 °C. The good performance and high thermal stability of 5% Ni/Al_2O_3 catalyst was probably related to the arrangement of the nickel particles, which resulted somehow thermally protected as partially embedded in the alumina carrier.

1. Introduction

The energy demand of the modern society stimulates exploration of new energy technologies. Partial oxidation is presently considered an alternative to steam reforming for the generation of H_2 from fossil fuels in decentralized applications [1]. Short contact time catalytic partial oxidation (SCT-CPO) of natural gas has received intensive attention because of its mild exothermic ability, high methane conversion, high selectivity towards CO and H_2 and a more compact plant technology. Moreover, the possibility to use air as oxidant appears a feasible route to reduce syngas production costs with certain technological advantages. An important recent example is the generation of H_2 for stationary or mobile fuel cells [2]. Moreover, the syngas obtained with SCT-CPO technology is characterized by H_2/CO values favourable for further downstream processes [3].

CPO of CH_4 has been largely discussed; several catalysts were proposed, including non-noble [4–14] and noble metals based ones [6,15–19]. The extensive work on SCT reactors [6,20–30] showed Rh as high active and selective, with a performance superior to that of other noble metals, able to avoid or, at least partially limit, coke formation [26]. The main chemical reactions involved in the catalytic process are represented in Eqs. (1)–(6):

Methane total oxidation (MTO):

$$CH_4 + 2O_2 \rightarrow CO_2 + 2H_2O \quad \Delta H^\circ_{298} = -802.3\ \text{kJ mol}^{-1} \tag{1}$$

Methane partial oxidation (MPO):

$$CH_4 + \tfrac{1}{2}O_2 \rightarrow CO + 2H_2 \quad \Delta H^\circ_{298} = -35.7\ \text{kJ mol}^{-1} \tag{2}$$

Methane steam reforming (MSR):

$$CH_4 + H_2O \rightarrow CO + 3H_2 \quad \Delta H^\circ_{298} = 206.2\ \text{kJ mol}^{-1} \tag{3}$$

Methane dry reforming (MDR):

$$CH_4 + CO_2 \rightarrow 2CO + 2H_2 \quad \Delta H^\circ_{298} = 247.3\ \text{kJ mol}^{-1} \tag{4}$$

Water gas shift equilibrium (WGS):

$$CO + H_2O \leftrightarrow CO_2 + H_2 \quad \Delta H^\circ_{298} = -41.1\ \text{kJ mol}^{-1} \tag{5}$$

Coke formation (Boudouard reaction):

$$2CO \rightarrow CO_2 + C \quad \Delta H^\circ_{298} = -72.9\ \text{kJ mol}^{-1} \tag{6}$$

It is widely accepted that with metal catalysts CH_4 is first oxidized to CO_2 and H_2O in the initial part of the catalytic bed until O_2

* Corresponding author. Tel.: +39 011 0904608; fax: +39 011 0904699.
E-mail address: stefania.specchia@polito.it (S. Specchia).

0920-5861/$ – see front matter © 2011 Elsevier B.V. All rights reserved.
doi:10.1016/j.cattod.2011.03.074

is exhausted [27]; then the reforming reactions of remaining CH_4 with steam and CO_2 initially formed occur [15,16]. This indirect mechanism, however, was proposed mostly through the observations of the temperature profile of catalysts bed. It was found that the catalyst temperature was significantly higher in the first part of the bed than in the latter one, caused by the initial exothermic combustion reactions followed by the endothermic reforming ones [28,29]. This phenomenon was present on different catalysts and under different reaction conditions [6]. However, at extremely high temperatures and very short contact time, a direct route syngas production was suggested [16,20,21]. Many researchers think that the reaction mechanism depends upon the types of catalyst used, in particular from both metal and support types and their chemical interactions [30]. Ultimately, the role of catalysts may be summarized as they all can be active for both partial and full oxidation, but the weight of each oxidation route is more sensitive and strictly linked to the individual catalyst.

Among the various noble metal catalysts examined in the literature, the Rh-based ones have been reported to be the most active and stable catalysts towards deactivation. However, Rh is a very expensive raw material, and its price fluctuates significantly. From 1992 up today it reached the following monthly average values: minimum of 209 US$ per troy oz on February 1997, maximum of 9776 US$ per troy oz on June 2008, and an actual of 2167 US$ per troy oz on August 2010 [31]. Cheaper and alternative metal-based catalysts (such as La-, Co-, and Ni-based ones) would be desirable. In particular, Ni based catalysts have been widely investigated because of their low cost and relatively high activity in methane CPO [8–10,12,16,32–36].

Dissanayake et al. [16] reported that 25% Ni/Al_2O_3 showed nearly complete conversion of methane with 95% CO selectivity at reaction temperatures above 700 °C. They found that the Ni/Al_2O_3 catalyst was deactivated by carbon deposition, and that overstoichiometric oxygen was needed to obtain a stable catalytic activity. In addition to coke formation, other drawbacks, such as sintering of Ni particles [32,36] and phase transformation of the support [33], have also been reported in the literature. Nonetheless, Ni-based catalysts have been widely studied because of their high CPO activity and economic advantages.

Aim of this work was the development of perovskite nickel-based catalysts for methane CPO to syngas in a self-sustained short contact time (SCT) reactor using pure oxygen. Their capability of maintaining the fixed bed temperatures lower than about 1200 °C independently of the operative weight hourly space velocity (WHSV) was pursued too; thus sintering and coking problems and the consequent performance decay could be minimized.

Various perovskites $LaNiO_3$-based catalysts were synthesized via Pechini method by substituting part of Ni with Co and part of Co with small atomic percentages of Pt. Their performance, in terms of CH_4 conversion, H_2 and CO selectivity and reactor temperature level, was compared to that obtained with 5% Ni/Al_2O_3 catalyst, prepared through incipient wetness impregnation over commercial alumina support using nickel nitrate as metal precursor.

The perovskites belonging to the family of $LaNiO_3$, doped with various transition and noble metals, have been deeply studied in the literature mainly for the dry reforming of methane [37–43] and autothermal reforming of methane [7,44], but only in a limited extension for the partial oxidation of methane [14,45].

Cobalt has been investigated as catalytic promoter in case of partial oxidation of methane: Co on Rh–Co/MgO catalysts improved the selectivity towards the direct partial oxidation route in the presence of gas-phase oxygen, but reduced the catalytic activity in the steam reforming of methane in the absence of oxygen [17]. The better performance related to the presence of Co was attributed to the greater methane dissociation and reduction degree during its partial oxidation [17]. On the contrary, the presence of Co on perovskites $LaNiO_3$ led to a decrease of the catalytic activity towards the dry reforming of methane [43], most probably due to the formation of the Co–Ni alloy.

2. Experimental

2.1. Catalysts preparation

The Ni–La-based perovskite catalysts were synthesized by Pechini method [46]. Firstly, $LaNiO_3$ was prepared; afterward, other catalytic perovskite materials were prepared by substituting part of Ni with Co and part of Co with small atomic percentages of Pt, obtaining the following five catalysts: $LaNiO_3$, $LaNi_{0.75}Co_{0.25}O_3$, $LaNi_{0.55}Co_{0.45}O_3$, $LaNi_{0.75}Co_{0.20}Pt_{0.05}O_3$ and $LaNi_{0.55}Co_{0.40}Pt_{0.05}O_3$. Metal nitrates of La, Ni, Co and Pt (97.7% minimum, Johnson Matthey) were used as precursors, together with citric acid monohydrate and ethylene glycol (all precursors from Sigma–Aldrich). Metal nitrates were dissolved in distilled water and then vigorously stirred at least for 15 min. Citric acid was then added in an amount equal to 5 times the moles of catalyst to be synthesized: the resulting solution was vigorously stirred for 20 min. After that, ethylene glycol was added to the previous solution, in a molar ratio 2:3 respect to citric acid. The so-obtained final solution was heated until 70 °C, and then stirred at the same temperature for 1.5 h until excess of water was vaporized and therefore a gel containing the metal cations inside a polymeric network was obtained. Finally, the gel was heated firstly at 2 °C min^{-1} till 300 °C, in order to burn the organic material; the obtained fine powder was placed in the refractory pot, heated at 2 °C min^{-1} to 800 °C and calcined at this temperature for 4 h in calm air.

Instead, 5% Ni/Al_2O_3 catalyst was prepared by Ni deposition over γ-Al_2O_3 irregular particles obtained by crushing and sieving commercial alumina spheres (3 mm in diameter, Sasol Germany GmbH); the fraction 600–1000 μm was used as support. Ni was deposited by incipient wetness impregnation technique at room temperature, using $Ni(NO_3)_2{\cdot}6H_2O$ dissolved in isopropyl alcohol (all precursors from Sigma–Aldrich). The as prepared particles were left at rest overnight and then placed in oven with a temperature ramp of 5 °C min^{-1} until 900 °C and calcined in calm air for 2 h [47].

2.2. Catalysts characterization

The as-prepared catalysts were characterized by different techniques: XRD (Seifert 3000P vertical diffractometer and nickel-filtered Cu Kα radiation with l = 0.1538 nm); XRF (Rigaku ZSX-100e with a 3 kW Rh tube); XPS (Escalab 200R spectrometer equipped with a hemispherical electron analyser and an Al Kα, with $h\nu$ = 1486.6 eV, 120 W X-ray source for the perovskite-based catalysts; PHI 5000 VERSA PROBE spectrometer equipped with a hemispherical electron analyzer and an Al Kα (with $h\nu$ = 1486.6 eV, 25.6 W X-ray source for the alumina-based catalyst); H_2-TPR (Micromeritics 2900); BET (Micromeritics ASAP 2100); HRTEM (JEOL-JEM 2100 *F* working at 300 kV); FESEM (FESEM FEI Quanta Inspect 200 LV apparatus, coupled with EDAX GENESIS SUTW sapphire detector).

The spent catalysts, i.e., after the catalytic tests below described, were further characterized by the following techniques: XRD, XRF, XPS, SEM-EDX, TGA-MS (Mettler-Toledo TGA analyser, equipped with a Balzers Quadstar 422 mass-spectrometer).

Concerning the XPS analysis, the area of the peaks was estimated by integration after peak smoothing and subtraction of an S-shaped background, and fitting of the experimental curve to a mixture of Lorentzian and Gaussian lines of variable proportions. All binding energies (BE) were referenced to the C 1s signal at 284.6 eV from

carbon contamination of the samples to correct the charging effects. Quantification of the atomic fractions on the sample surface was obtained by integration of the peaks with appropriate corrections for sensitivity factors [48].

The specific surface area (SSA) was measured via N_2 adsorption, at the liquid N_2 temperature by degassing in vacuum for at least 12 h at 150 °C before analysis. The SSA was determined by applying the BET equation within the relative pressure range 0.05–0.3.

H_2-TPR analyses of the as-prepared perovskites were carried out in a U-shaped quartz reactor to assess the reducibility of the catalysts. Prior to the reduction tests, each sample (30 mg) was flushed with He at 110 °C for 15 min and then cooled down to room temperature. TPR profiles were obtained by heating the sample under a 10% H_2/Ar flow (50 N mL min^{-1}) from 30 to 1000 °C at a rate of 10 °C min^{-1}.

TGA-MS was used to assess both the thermal stability of the spent catalysts and the possible presence of carbonaceous residues in the catalysts after the activity tests. Samples of each spent catalysts (80–140 mg in weight) were treated in the TGA analyser up to 1000 °C at a constant rate of 10 °C min^{-1} when flowing both chromatographic air (50 N mL min^{-1}) and argon (50 N mL min^{-1}). The gas stream generated during TGA analysis was sent to a mass spectrometer to measure the various compounds concentration, in particular H_2O and CO_2.

2.3. Catalytic activity tests

The catalytic activity of the prepared catalysts was determined in a fixed bed reactor, already fully described in [49,50]. Briefly, CH_4 and O_2, mixed at room temperature, were fed to the reactor (Inconel 601 tube, 15 mm i.d., 2 mm wall thickness, with the internal surface covered by a layer of oxidized FeCrAlloy to avoid any contact between the reactive gases and the Inconel wall, just to prevent any catalytic effect of Ni present in the latter). For safety reasons, pure N_2 (technical grade, rate 2 N l min^{-1}) was used to wash and fill up the reactor before and after each test. The catalyst fixed bed was arranged between two inert fixed beds: upstream, quartz particles (to complete feed static mixing) followed by high thermal conductivity SiC particles, to provide a shield for the radiant energy emerging from the catalytic zone and promote reagents preheating. Downstream, low thermal conductivity quartz particles reduced the heat losses and cooled slowly the outlet stream. The gas temperatures were monitored by thermocouples located at catalytic bed inlet and outlet. The outlet gas stream composition was determined by a hygrometer (GE), for humidity, and by a multiple gas analyzer (ABB), for the concentrations of H_2 (thermal conductivity analyzer, module Caldos 17), CO/CO_2/CH_4 (infrared analyzer, module Uras 14), and O_2 (paramagnetic O_2 analyzer, module Magnos 106). All the collected data, in terms of gas stream concentrations, inlet and outlet temperatures (T_{in} and T_{out}, respectively), were recorded when the steady-state condition was reached. For safety and environment protection reasons, after the analysis section, the produced syngas was completely oxidized in a catalytic honeycomb burner.

The reactor was heated up to 920 °C in a tubular oven by feeding N_2 (2 N l min^{-1}). Then, the CPO reaction was ignited feeding a room temperature mixture of pure CH_4 and O_2 at O_2/CH_4 ratio always equal to 0.57 (15% above the stoichiometry [49,50]). No diluent balance gas was fed in the reactor. Once ignited the catalytic bed, the oven was switched off as the SCT-CPO reaction resulted thermally self-sustained by the heat released in the reaction zone. The ignition procedure was very quick taking about 1 min. The feed flow rate was adjusted accordingly to increase the WHSV from 130 to 560 N l h^{-1} g_{cat}^{-1}. The prepared catalysts were tested by placing in the reactor 1.5 g, to form a fixed bed with about 2 cm of axial length.

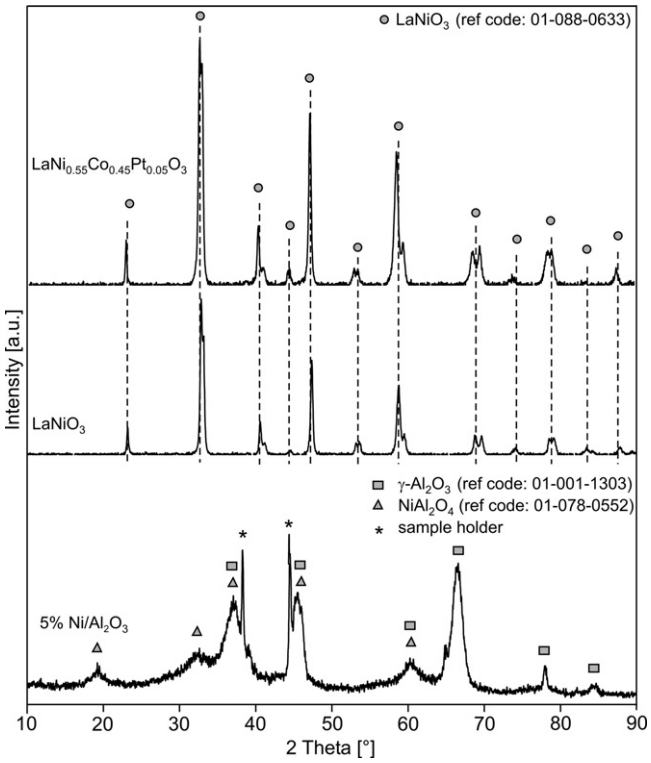

Fig. 1. XRD spectra of the as-prepared $LaNiO_3$, $LaNi_{0.55}Co_{0.40}Pt_{0.05}O_3$ and 5% Ni/Al_2O_3 catalysts.

3. Results

3.1. Characterization of the fresh catalysts

The XRD analyses performed on all calcined Pechini's perovskites catalysts, included the partially substituted ones, showed that the characteristic $LaNiO_3$ perovskite with rhomboedral structure was formed in all samples, with a good degree of crystallinity, without the formation of other undesired solid phase. No segregated phases different from the $LaNiO_3$ perovskite, in fact, were found in the pattern of all the substituted samples, indicative of the high degree of incorporation of the La, Ni and Co into the perovskite structure achieved with the Pechini preparation method. Peaks belonging to Pt species were not detected. The obtained spectra indicated, moreover, that the employed calcination temperature was appropriate to develop the perovskite phase where both cations in B position, Co^{3+} and Ni^{3+}, were incorporated in a homogeneous lattice distribution. Such a result was absolutely comparable to those obtained by de Araujo et al. [45] on $LaNi_{1-x}Co_xO_3$ perovskites. Fig. 1 shows, as an example, the recorded spectra of $LaNiO_3$ and $LaNi_{0.55}Co_{0.40}Pt_{0.05}O_3$ catalysts. The XRD spectrum of 5% Ni/Al_2O_3 catalyst, also visible in Fig. 1, revealed the presence of the phase γ of Al_2O_3 and the spinel $NiAl_2O_4$. No other Ni-based structures were detected. Such a result was in agreement with those obtained by Dissanayake et al. [16] on 25% Ni/Al_2O_3.

In the XPS analysis of the perovskite-based catalysts (see, as an example, Fig. 2 for $LaNi_{0.55}Co_{0.45}O_3$), the La 3d level was characterized by a double peak for each spin–orbit component, attributed to energy loss phenomena (shake-up satellites) induced by intense O 2p → La 4f charge transfer events or due to strong final state mixing of electronic configurations [51]. La 3d peak positions observed for the $LaNiO_3$ were in agreement with the literature data for La^{3+} in La_2O_3 with an energy value equal to 834 eV for La $3d_{5/2}$ and were not modified by the addition of Co and Pt in the perovskite structure. Ni 3p spectra region were analyzed since La 3d superimposed on Ni

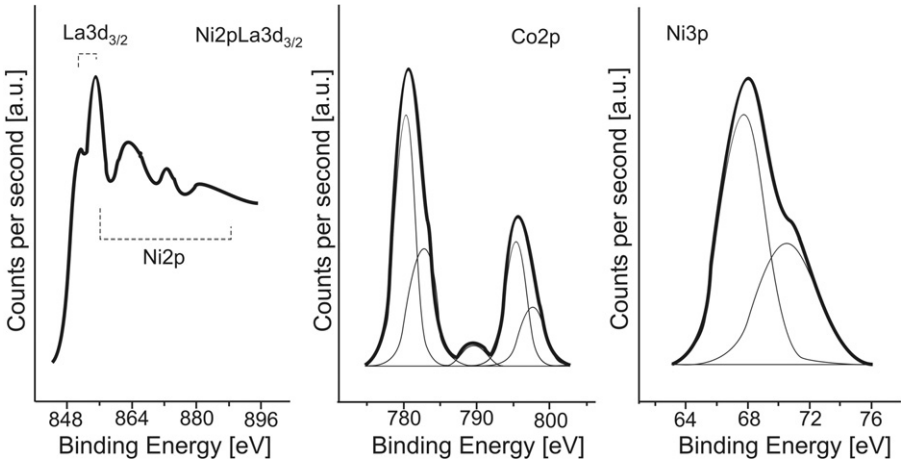

Fig. 2. XPS spectra of the regions La 3d, Co 2p and Ni 3p for the as-prepared $LaNi_{0.55}Co_{0.45}O_3$ catalyst.

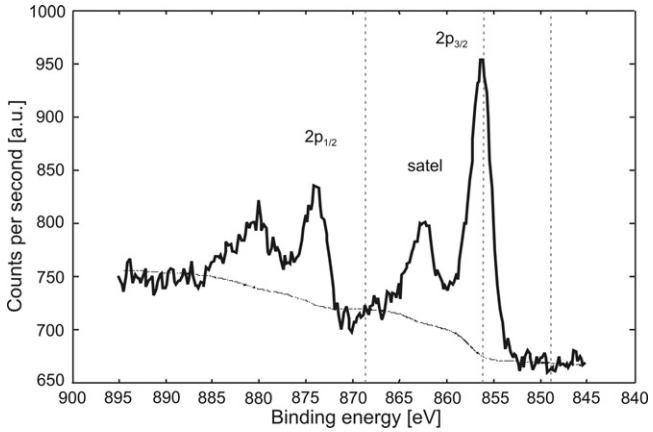

Fig. 3. XPS spectrum of the Ni 2p region for the 5% Ni/Al_2O_3 catalyst.

2p spectra (Fig. 2). The peak position, the atomic fraction (reported in Table 1) and the energy separations for both peaks confirmed the presence of a clear perovskite structure.

In the XPS analysis of calcined 5% Ni/Al_2O_3 catalyst, as shown in Fig. 3, Ni 2p core-level spectra were investigated. The Ni $2p_{2/3}$ binding energy was 856.2 eV (±0.3 eV): even though the values in the literature for the Ni 2p binding energies are spread over a fairly broad energy interval, this can be assigned to nickel aluminate $NiAl_2O_4$. This result was fully in agreement with the XRD spectrum of 5% Ni/Al_2O_3. Moreover, the Ni $2p_{1/2}$–Ni $2p_{3/2}$ splitting of 17.8 eV confirmed this assignment, and the presence of strong shake-up satellite structures indicated the presence of Ni^{2+} ions in a paramagnetic state [52]. In fact, the as-prepared fresh catalyst particles appeared light blue-green like spinel $NiAl_2O_4$. Therefore, the spinel $NiAl_2O_4$ structure could be present on the catalyst surface, in agreement with the findings of Dissanayake et al. [16], which evidenced by XPS analysis the presence of such a spinel in the near-surface region thanks to the Ni $2p_{3/2}$ peak at a binding energy of 856 eV, with an accompanying shake-up satellite peak at 862 eV, for a 25% Ni/Al_2O_3 catalyst for CPO reaction. Moreover, this occurrence could be supported considering the used preparation method (in particular, the calcination step at 900 °C for 2 h) which could have created a stronger bonding between Ni and the Al_2O_3 carrier.

Almost all the surface atomic ratios Ni/La, Co/La and Pt/La calculated from the XPS analysis in the perovskite-based catalysts were slightly higher than the stoichiometric values (see Table 1). On the contrary, the sample 5% Ni/Al_2O_3 presented a surface Ni/Al atomic ratio almost twice the stoichiometric ratio, denoting thus an enrichment of Ni on the surface of the alumina particles.

On this point of view, FESEM analysis of the as-prepared 5% Ni/Al_2O_3, shown in Fig. 4, enlightened at high magnification a catalyst morphology characterized by long and narrow leaf-shape superficial configurations. The EDX analysis related to all the areas shown in the two pictures was reported in Fig. 4 as subsurface atomic ratios (the EDX beam penetrates for about 1 μm). In particular, the Ni/Al values enlightened areas with different Ni local loads, anyway with an average value in a good agreement with that determined by XPS analysis (see Table 1). The EDX analysis

Table 1
BET specific surface area, surface atomic ratios (from XPS analysis) and subsurface atomic ratios (from XRF analysis) of all the nickel-based catalysts.

Catalysts	BET SSA ($m^2\ g^{-1}$)		Ni/La AR	Co/La AR	Pt/La AR	Ni/Al AR
$LaNiO_3$	2.8	XPS	1.15	–	–	–
		XRF	0.94	–	–	–
$LaNi_{0.75}Co_{0.25}O_3$	2.6	XPS	0.85	0.23	–	–
		XRF	0.75	0.24	–	–
$LaNi_{0.55}Co_{0.45}O_3$	14.1	XPS	0.63	0.39	–	–
		XRF	0.56	0.42	–	–
$LaNi_{0.75}Co_{0.20}Pt_{0.05}O_3$	3.1	XPS	0.93	0.24	0.10	–
		XRF	0.77	0.20	0.05	–
$LaNi_{0.55}Co_{0.40}Pt_{0.05}O_3$	2.8	XPS	0.64	0.37	0.09	–
		XRF	0.55	0.38	0.05	–
5% Ni/Al_2O_3	117.2	XPS	–	–	–	0.09
		XRF	–	–	–	0.04

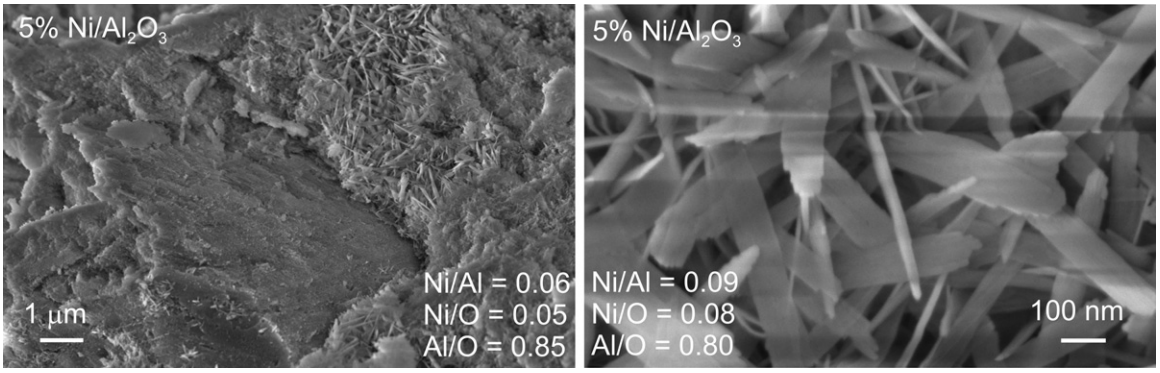

Fig. 4. FESEM images and EDX analysis of the 5% Ni/Al_2O_3 catalyst.

related to areas of few squared μm confirmed an average Ni load on the external surface (calculated from various measurements) equal to 10.6% by weight whereas the same analysis performed on the cross-section of a cut particle disclosed an average Ni load decreasing from the outer surface to the particle centre, proving, consequently, the existence of a nickel gradient from outside to the core of the supported catalyst particles: in fact, the load in the centre was equal to approx. 5.1%. Practically, part of the deposited Ni resulted embedded in the alumina matrix.

HRTEM images on perovskite-based catalysts, shown in Fig. 5 for $LaNi_{0.75}Co_{0.25}O_3$ and $LaNi_{0.75}Co_{0.20}Pt_{0.05}O_3$, pointed out the presence of irregular aggregates constituted by nanometric particles. All the catalysts prepared with Pechini showed HRTEM pictures very similar to those in Fig. 5. The performed EDX analysis (reported in Fig. 5) confirmed the preparation of quite homogeneous catalysts; the calculated Ni/Al, Ni/La and Co/La subsurface atomic ratios were slight lower compared to the values of the surface atomic ratios estimated by XPS analysis (see Table 1). The present HRTEM pic-

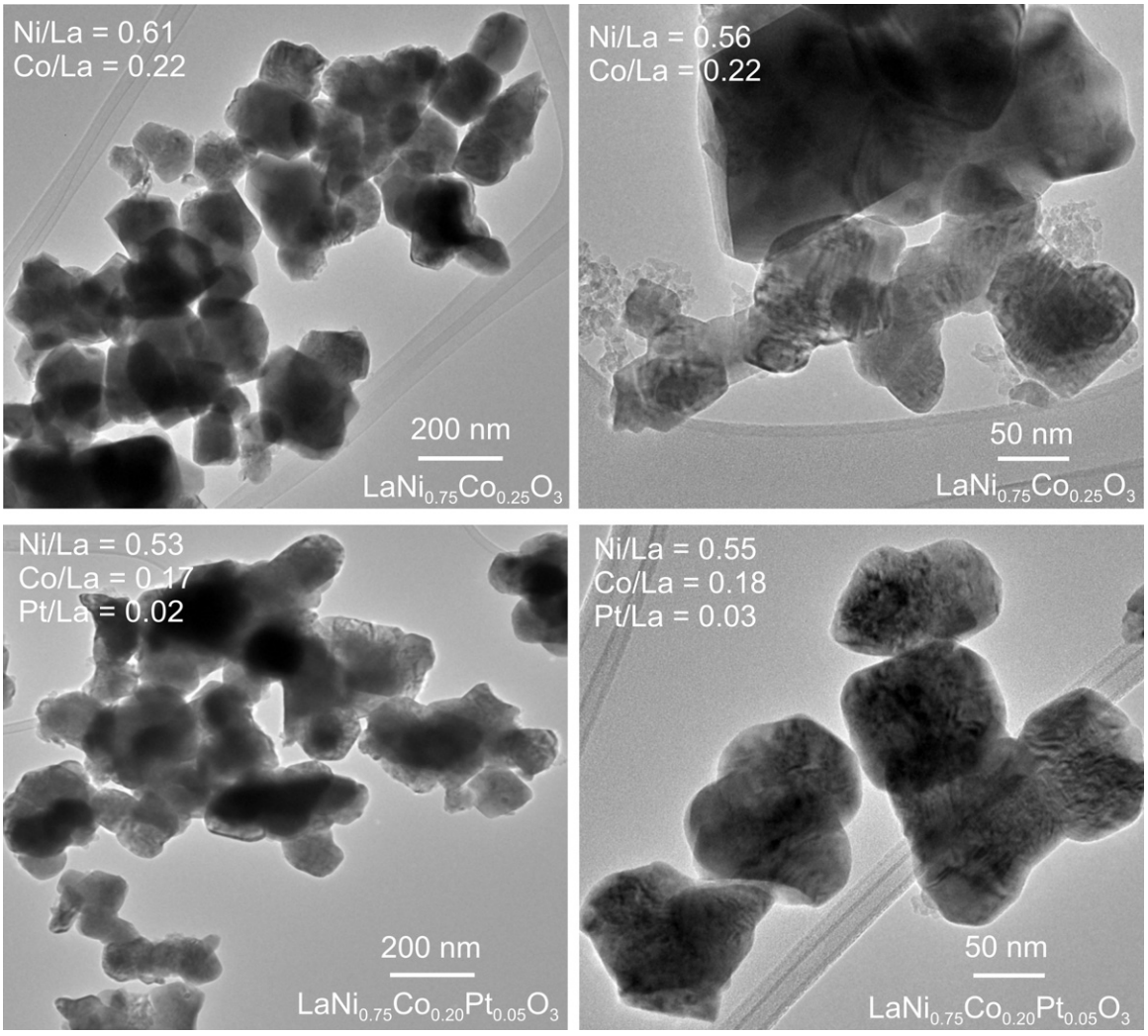

Fig. 5. HRTEM images and EDX analysis of the $LaNi_{0.75}Co_{0.25}O_3$ (top strip) and $LaNi_{0.75}Co_{0.20}Pt_{0.05}O_3$ (bottom strip).

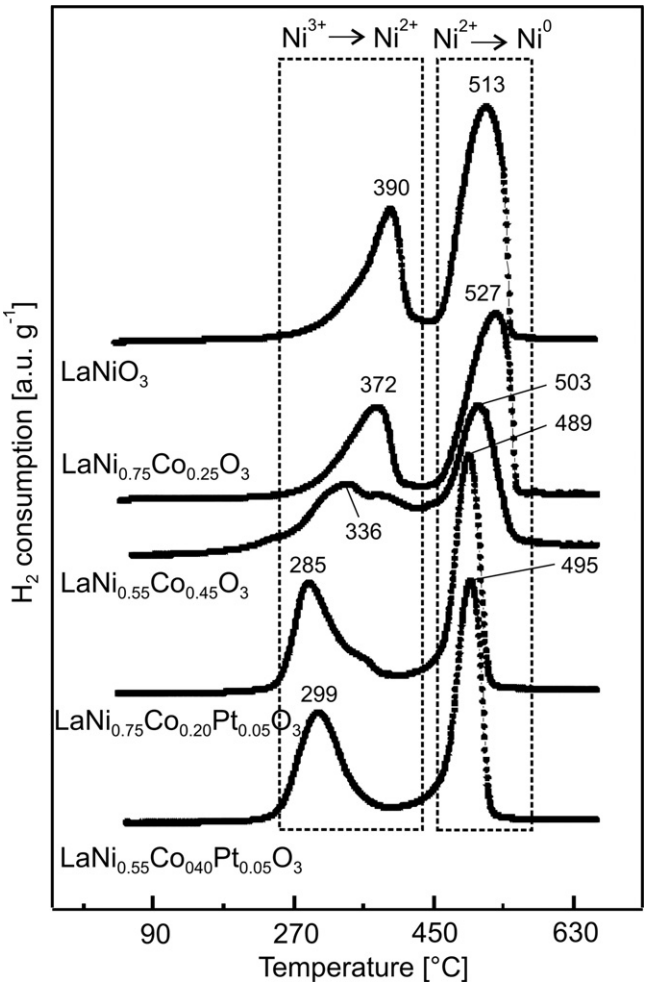

Fig. 6. H_2-TPR profiles of the as-prepared perovskite catalysts.

tures were very similar to those reported in the literature for $LaNiO_3$ prepared by explosion method [37], gel combustion technique [53] and reverse micro-emulsion [54].

The XRF analysis performed on the as-prepared perovskite samples revealed slightly lower values of Ni/La, Pt/La and Ni/Al atomic ratios (see Table 1), more similar to the values obtained by EDX analysis (reported in Figs. 4 and 5). Considering that XRF and EDX analysis have much higher penetration depth compared to XPS analysis, the results coming from the former ones can be considered as subsurface (or bulk) atomic ratios; therefore, the lower atomic ratio measured by XRF and EDX analyses, in particular for the Ni/La and Pt/La ratios, could denote a possible enrichment of Ni and Pt on the catalysts' surface. The Co/La ratio values, instead, were higher when calculated from the XRF, except than for the $LaNi_{0.75}Co_{0.20}Pt_{0.05}O_3$ perovskite. Possibly, Co showed the tendency to go deep in the core of the particles. As also noticed by Villoria et al. [55] for $LaCoO_3$ perovskites, the Co/La values were mostly slightly lower than the corresponding stoichiometric ones: in accordance with previous works [56,57], such lower values could be attributed to the segregation of La^{3+} ions to the surface due to their basicity. As opposite compared to the value obtained by XPS analysis, the Ni/Al subsurface atomic ratio estimated by XRF analysis for the 5% Ni/Al_2O_3 catalyst was closer to the stoichiometric value (equal to 0.043). Consequently, Ni presented decreasing concentration gradient from the surface to inside particles, anyway confined in a surface layer of a very small thickness.

The SSA values (reported in Table 1) of the perovskite-based catalysts were similar among them and very low (with the exception of $LaNi_{0.55}Co_{0.45}O_3$, which presented a higher value). These low values can be considered characteristic of materials synthesized according to the Pechini method. Besides, no regular change of these values with the substitution degree of Co and Pt was observed, in agreement with de Araujo et al. [45]. On the contrary, 5% Ni/Al_2O_3 catalyst presented a SSA value two orders of magnitude higher, 117.2 $m^2\,g^{-1}$.

Basically, H_2-TPR profiles of the perovskite samples, presented in Fig. 6, showed that a reducing environment led to the formation of a structure containing La_2O_3 and metallic Ni, as demonstrated also in the literature for the $LaNiO_3$ perovskite exposed to reducing conditions [7]. Moreover, the H_2-TPR profiles were found to be dependent on the Co and Pt substitution degree. The starting sample $LaNiO_3$ exhibited a first reduction peak at 390 °C, which accounted for the reduction of Ni^{3+} into Ni^{2+} species, and a second peak at 513 °C belonging to the formation of metallic nickel [45]. For the partially substituted samples, the presence of only Co shifted the second peak (the high temperature one) to a slightly higher temperature for $LaNi_{0.75}Co_{0.25}O_3$, in agreement with the literature data [14,43,45], and to a slightly lower temperature for $LaNi_{0.55}Co_{0.45}O_3$. On the contrary, the first peak (the low temperature one) shifted to slightly lower temperatures. As concerns the presence of both Co and Pt in the perovskite structure, this situation provoked the decrease of both the high and the low temperature peaks. The formation of Ni metallic particles on a La_2O_3 matrix after reduction treatment was also observed by Sierra Gallego et al. [40,43] and de Lima et al. [44]. Ni^0 on La_2O_3 is known to be a stable and active catalyst for steam reforming and oxidative steam reforming of hydrocarbons: such a catalyst can also be prepared by activating under H_2-stream the $LaNiO_3$ perovskite used as precursor [44]. No peaks associated with the reduction of oxidized Pt were noticed for the two Pt-containing samples: perhaps, Pt was already reduced prior to the TPR analysis.

3.2. Catalytic activity tests

The main results from the catalytic activity tests carried out on all synthesized catalysts are shown as a function of WHSV in terms of CH_4 conversion (Fig. 7), H_2 selectivity (Fig. 8), CO selectivity (Fig. 9), and T_{in} and T_{out} (Fig. 10). A comparison with the 5% Ni/Al_2O_3 catalyst is presented, too. As a general comment, the global performance of the latter appeared unequivocally superior then those of the perovskite-based catalysts.

Looking at the CH_4 conversion results (Fig. 7), the best catalytic performance belonged to 5% Ni/Al_2O_3: it remained in the very narrow range of 86–90%, independently of the WHSV values, with a regular and uniform trend. On the contrary, for the perovskite-based catalysts CH_4 conversion varied in a wide range (40–80%), always decreasing with the increase of the WHSV. The partial substitution of Ni with Co worsened the conversion, whereas the further substitution of Co with small Pt amount showed for $LaNi_{0.55}Co_{0.40}Pt_{0.05}O_3$ a CH_4 conversion higher also than that of the not-substituted $LaNiO_3$ perovskite catalyst, at least for WHSV < 320 N l h^{-1} $g_{cat}{}^{-1}$. The lower value of the surface atomic Pt/La ratio in the fresh status (compared to that of $LaNi_{0.75}Co_{0.20}Pt_{0.05}O_3$) could be responsible of a higher Pt exposition on the catalyst surface and hence of the slightly improved performance.

The 5% Ni/Al_2O_3 catalyst showed also the best results in terms of H_2 selectivity (Fig. 8), presenting values (90–93%) practically constant with WHSV. Among the perovskite materials, the $LaNi_{0.75}Co_{0.20}Pt_{0.05}O_3$ catalyst presented the best H_2 selectivity, which was decreasing with WHSV from 70% to 49% at around 400 N l h^{-1} $g_{cat}{}^{-1}$.

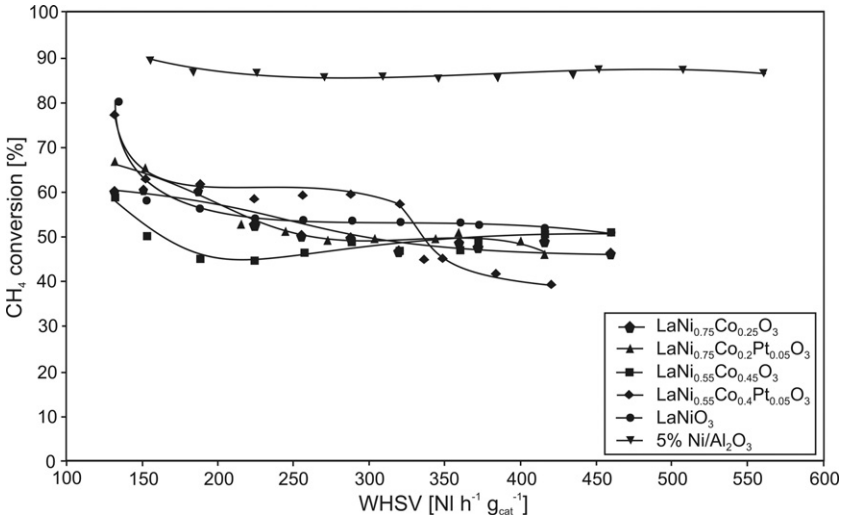

Fig. 7. CH_4 conversion vs. WHSV for all the synthesized nickel based catalysts tested in the SCT-CPO reactor.

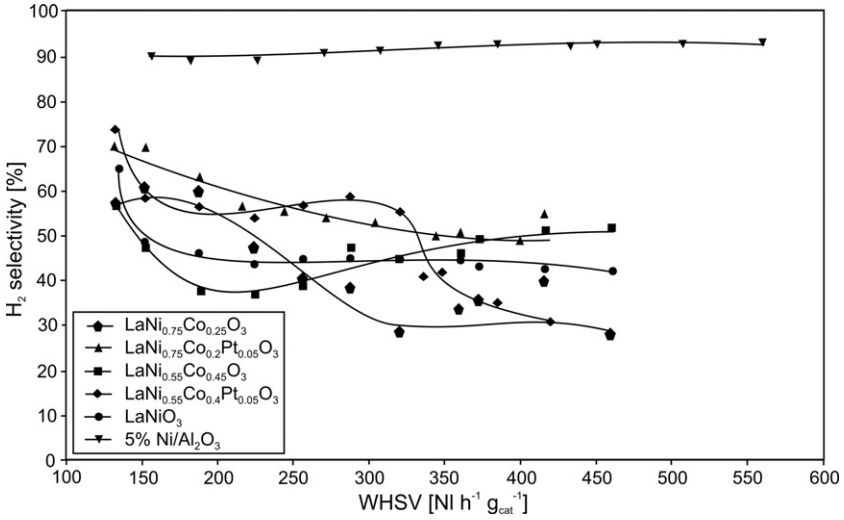

Fig. 8. H_2 selectivity vs. WHSV for all the synthesized nickel based catalysts tested in the SCT-CPO reactor.

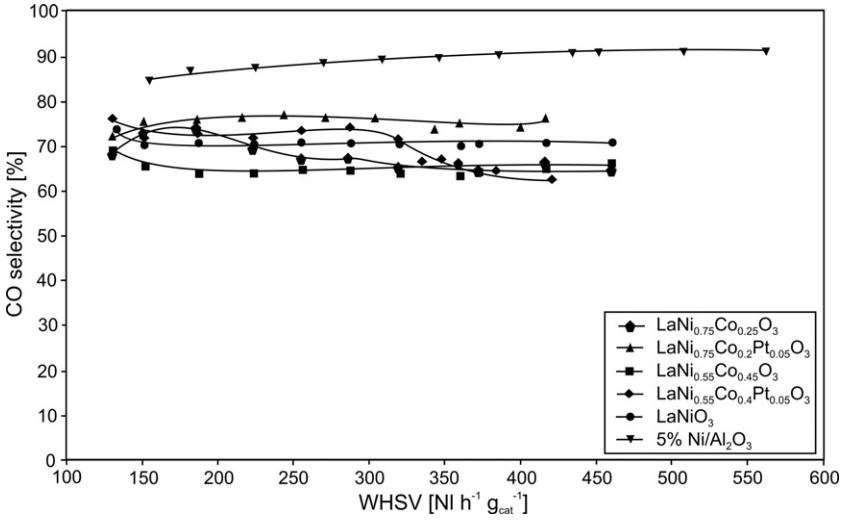

Fig. 9. CO selectivity vs. WHSV for all the synthesized nickel based catalysts tested in the SCT-CPO reactor.

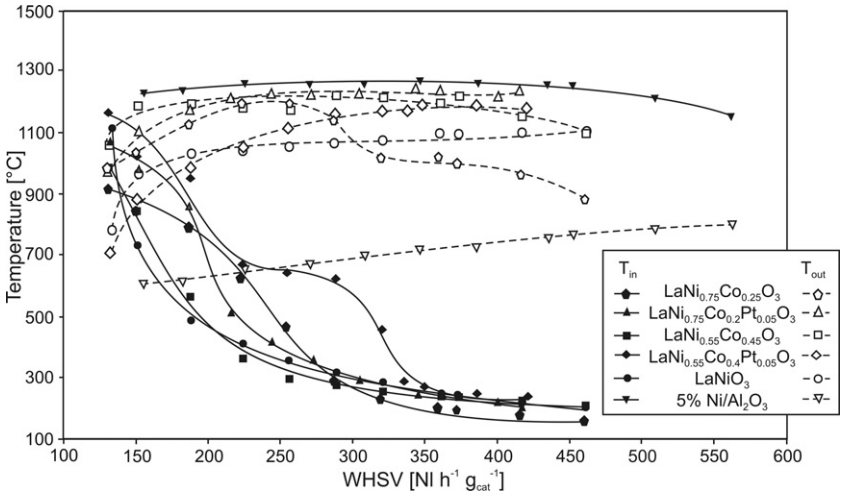

Fig. 10. T_{in} and T_{out} temperatures vs. WHSV for all the synthesized nickel based catalysts tested in the SCT-CPO reactor.

By comparing the CO selectivities (Fig. 9), 5% Ni/Al_2O_3 catalyst exhibited again the highest values, slightly increasing from 86% to 91% by increasing WHSV. All the perovskite-based catalysts were characterized by CO selectivity values less dispersed than the corresponding CH_4 conversion and H_2 selectivity values, showing thus the tendency in a larger CO production rather than in H_2, compared to the 5% Ni/Al_2O_3 catalyst.

Furthermore, with all the perovskite-based catalysts, when during the catalytic activity tests the WHSV was reduced down from the higher to the lower tested value, the recorded CH_4 conversion, H_2 and CO selectivity values were lower compared to the corresponding ones recorded when WHSV was moving from the lower to the higher tested value. On the contrary, the overall performance of 5% Ni/Al_2O_3 catalyst remained practically constant by increasing and/or decreasing WHSV.

Analysing the inlet and outlet temperatures of the fixed bed, recorded during the activity tests, shown in Fig. 10, all the perovskite-based catalysts presented the same behaviour: at low WHSV values T_{in} was higher than the corresponding T_{out}. By increasing WHSV, T_{in} significantly decreased and T_{out} increased till about 1200 °C; there was a negative ΔT difference ($T_{in} - T_{out}$), reaching the value of approx. −850 °C in the worst case, for catalyst $LaNi_{0.55}Co_{0.45}O_3$. On the contrary, T_{in} and T_{out} of 5% Ni/Al_2O_3 showed very different trends: T_{in} was very stable and constant by varying WHSV (either increasing or decreasing), and always higher than the corresponding T_{out}, therefore with positive ΔT values varying from around 550 °C at the lowest to around 300 °C at the highest tested WHSV (see Fig. 10). The found ΔT trend within the catalytic bed allowed supposing that 5% Ni/Al_2O_3 catalysts favoured the indirect reaction mechanism, characterized by the coexistence of two reaction zones: a first zone at the entrance of the catalytic bed with strongly exothermic CH_4 combustion to H_2O and CO_2 (combustion zone), followed by a second zone with strongly endothermic steam- and CO_2-reforming downstream (reforming zone) [16,22]. The perovskite-based catalysts instead, demonstrated an opposite effect: they were not able to promote the exothermic reactions in the catalytic bed inlet zone at very short residence time, therefore the combustion zone shifted to the final part of the catalytic bed, so with a limited catalytic volume for carrying on the reforming reactions.

On the best catalyst, i.e., 5% Ni/Al_2O_3, the activity test run by varying WHSV was repeated a second time, for a total of approx. 16 h of operative work for the catalytic bed (each run from the lowest to the highest WHSV and coming back to the lowest WHSV tested took approx. 8 h), to verify the catalytic stability with time on stream. This period of time is not a long one, anyway, it can be considered sufficiently indicative of the bed capability towards any sintering or deactivation effects due to the very high temperature level supported by the catalytic material during the tests. The results in terms of CH_4 conversion and H_2 selectivity are reported in the comparative histograms of Fig. 11 for the minimum, medium and maximum WHSV values. All the results obtained at the other WHSV values were in line with those reported in Fig. 11. The performance of the catalyst was maintained at very good levels, with a very limited loss: on average, CH_4 conversion slightly decreased up to ∼3%, whereas the H_2 selectivity decreased up to ∼6.5%. Similar results were obtained with durability tests on Rh/Al_2O_3 catalysts with Rh embedded in the alumina matrix [58]: with ageing, a slight decrease of CH_4 conversion and H_2 selectivity were, in fact, observed. The stable performance of the embedded catalysts during methane partial oxidation could be linked to the protection offered by the surrounding layer of Al_2O_3, which prevented extensive sintering of the active metal phase, even after the attainment of high temperatures in the fixed bed [59].

3.3. Characterization of the spent catalysts

After the catalytic activity test runs, a further characterization on the spent catalysts was carried out to better understand what happened, in particular to the perovskite-based catalysts.

A new series of XRD spectra is shown in Fig. 12. The diffraction profiles of the perovskite-based catalysts after only one test in the SCT-CPO reactor showed that the initial perovskite structure collapsed to form mainly La_2O_3, as shown in Fig. 12 for $LaNiO_3$ and $LaNi_{0.55}Co_{0.45}O_3$ catalysts, just as examples. Moreover, other structures as the spinel La_2NiO_4 and the hydroxide $La(OH)_3$ appeared in a lesser extent, so as metallic Ni, and Ni and Co oxides (the latter only for the Co-substituted perovskites). The production of the lanthanum hydroxide was attributed to the hydroxylation of La_2O_3 present in the sample upon exposure to atmospheric humidity (or steam-containing atmospheres), according to the mechanism described by several authors [14,60]. In some cases, also the $La_2O_2CO_3$ carbonate was detected (see diffraction profile of $LaNi_{0.55}Co_{0.45}O_3$). No Pt-based compounds, neither carbonaceous residues, were detected. Compounds as $La(OH)_3$ and $La_2O_2CO_3$ were evidenced by XRD analysis of La-based perovskites also by other authors in the literature [14,55,61]. The presence of La_2O_3, Ni^0, NiO and CoO was absolutely compatible with the

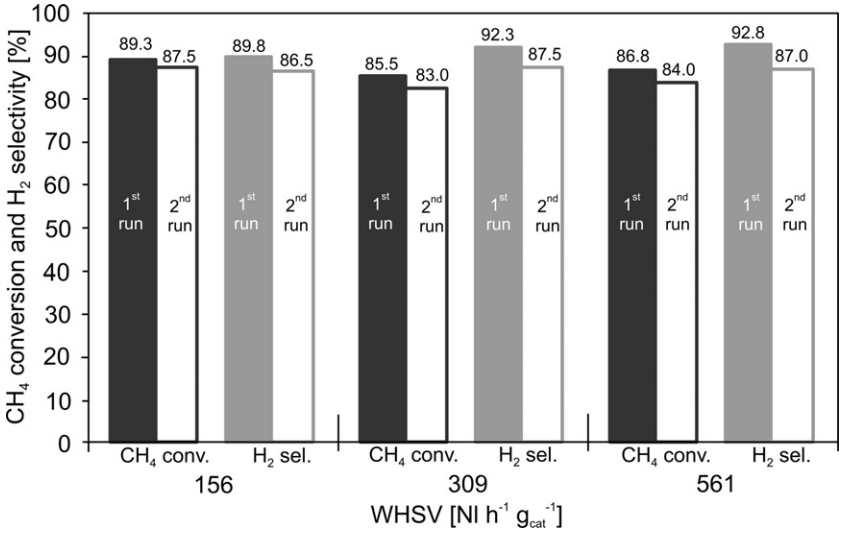

Fig. 11. CH_4 conversion and H_2 selectivity at min/average/max WHSV obtained in the 1st and 2nd catalytic activity test runs on SCT-CPO reactor for the 5% Ni/Al_2O_3 catalyst.

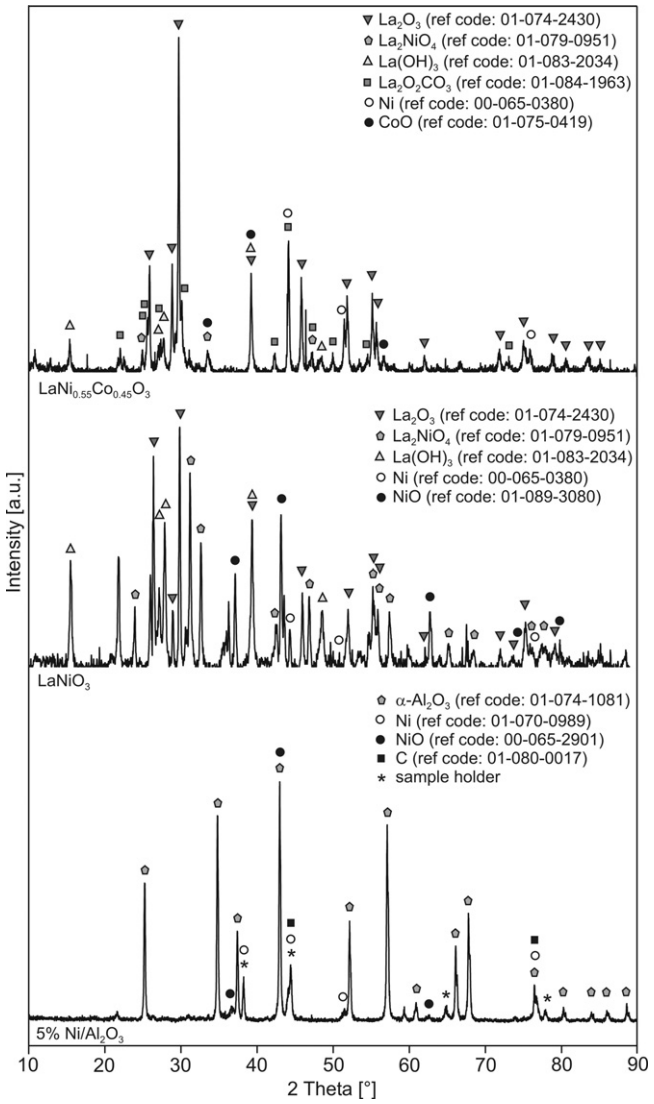

Fig. 12. XRD spectra of $LaNiO_3$ and $LaNi_{0.55}Co_{0.45}O_3$ perovskites catalyst after the 1st catalytic activity test run and of 5% Ni/Al_2O_3 after the 2nd catalytic activity test run on SCT-CPO reactor.

reducibility of the perovskite-based catalyst in a reducing environment, as the CPO process is, and already demonstrated also by the TPR analysis of the fresh samples (see Fig. 6), and in agreement with the literature data [14,40,45].

The XRD pattern of the spent 5% Ni/Al_2O_3 catalyst (at the end of the 2nd test run) presented the transformation of the alumina from γ- to α-phase. Moreover, the spinel $NiAl_2O_4$ (present on the fresh as-prepared sample, see Fig. 1) was not anymore present, but peaks belonging to Ni^0 and NiO appeared. Such a result was in agreement with the findings of Dissanayake et al. [16]. Furthermore, on this catalyst some peaks belonging to C with cubic structure appeared as well. XPS analysis performed on the spent 5% Ni/Al_2O_3 catalyst (not reported here) confirmed the presence of NiO species: the prominent Ni $2p_{3/2}$ peak shifted to lower value at a binding energy of 854.6 eV (±0.3 eV), thus confirming that the form of Ni in the near surface region (i.e., the uppermost 2–5 nm layer) was principally NiO.

The SSA values measured on 5%Ni/Al_2O_3 after the second activity test run resulted much lower ($4.1\ m^2\ g^{-1}$) compared to that determined on the freshly prepared catalyst. The drop in this SSA value by one order of magnitude was probably due to the transformation at the high reaction temperature of the initial γ-Al_2O_3 phase towards α-Al_2O_3 one, as confirmed by the XRD analysis carried out on 5% Ni/Al_2O_3 at the end of the second CPO test run (see XRD spectrum in Fig. 12). The alumina phase transformation was attributed to the high temperature reached within the fixed bed: despite the maximum recorded temperature at the fixed bed inlet did not exceed 1250 °C, certainly, the temperatures inside the fixed bed were higher, as demonstrated by other authors [62,63].

Also the XPS analysis (whose spectra are not presented) was performed on the spent 5% Ni/Al_2O_3 catalyst. The Ni/Al surface atomic ratio decreased from 0.09 (see Table 1) to 0.06 (see Table 2). Moreover, the XPS revealed the presence of C, which was accounted as C/Al surface atomic ratio of 0.24.

New XRF investigations on all the spent catalysts allowed calculating the subsurface atomic ratios reported in Table 2. In opposition to the XPS analysis, the spent 5% Ni/Al_2O_3 catalyst presented a huge increase of the subsurface Ni/Al atomic ratio, as if Ni resulted embedded in the alumina matrix. Instead, for $LaNiO_3$ and $LaNi_{0.75}Co_{0.25}O_3$ perovskites, the Ni/La subsurface atomic ratios slightly increased compared to the corresponding values in the fresh status (compare Table 1 with Table 2). On the contrary, on the perovskites with Ni partially substituted with Co and Pt the Ni/La

Table 2
Subsurface atomic ratios (from XRF and EDX analysis) of all the spent nickel-based catalysts and surface atomic ratios (from XPS analysis) of the spent 5% Ni/Al_2O_3 catalyst only.

Catalysts		Ni/La AR	Co/La AR	Pt/La AR	Ni/Al AR	C/La (C/Al) AR
$LaNiO_3$	XRF	1.08	–	–	–	–
$LaNi_{0.75}Co_{0.25}O_3$	XRF	0.76	0.29	–	–	–
	EDX	1.06	0.32	–	–	0.18
$LaNi_{0.55}Co_{0.45}O_3$	XRF	0.45	0.42	–	–	–
$LaNi_{0.75}Co_{0.20}Pt_{0.05}O_3$	XRF	0.69	0.20	0.05	–	–
	EDX	0.61	0.17	0.04	–	0.12
$LaNi_{0.55}Co_{0.40}Pt_{0.05}O_3$	XRF	0.51	0.40	0.05	–	–
5% Ni/Al_2O_3	XRF	–	–	–	0.19	–
	EDX	–	–	–	0.06	(0.05)
	XPS	–	–	–	0.06	(0.24)

subsurface atomic ratios slightly decreased compared to the corresponding values in fresh conditions. The subsurface Co/La atomic ratios varied without any apparent relationship with the substitution degree, whereas the subsurface Pt/La atomic ratios remained constant.

SEM-EDX analyses were performed on some of the spent catalysts. The obtained results, in terms of subsurface atomic ratios are reported in Table 2. The spent 5% Ni/Al_2O_3 catalyst presented a subsurface Ni/Al atomic ratio of 0.06, which was compatible with the recorded increase of the surface atomic ratio calculated by XPS analysis. A back-scattered picture of this sample is reported in Fig. 13: the bright particles were Ni clusters. Also for this sample the EDX detected the presence of C: the corresponding subsurface C/Al atomic ratio, was equal to 0.05, much lower compared to the surface one calculated by XPS analysis (equal to 0.24), sign that the deposited carbonaceous residues were mainly on the catalyst's surface. For the perovskite-based catalysts, $LaNi_{0.75}Co_{0.25}O_3$ presented a slight increase of all the subsurface atomic ratios, whereas the catalyst $LaNi_{0.75}Co_{0.25}Pt_{0.05}O_3$ presented a slight decrease of these values. The EDX analysis revealed the presence of the corresponding subsurface atomic ratios are reported in Table 2.

TGA-MS analyses were performed to quantify the carbonaceous residues deposited on the catalysts after the activity test runs, and to deeply analyze the phase changes on each sample. Fig. 14 shows the evolution of the mass of each used sample as a function of the temperature under a chromatographic air flow (black curves) or under an argon flow (gray curves). Fig. 15 presents the correlated H_2O and CO_2 emissions curves obtained with the mass spectrometer for each performed TGA analysis (in chromatographic air: black curves; in argon: gray curves).

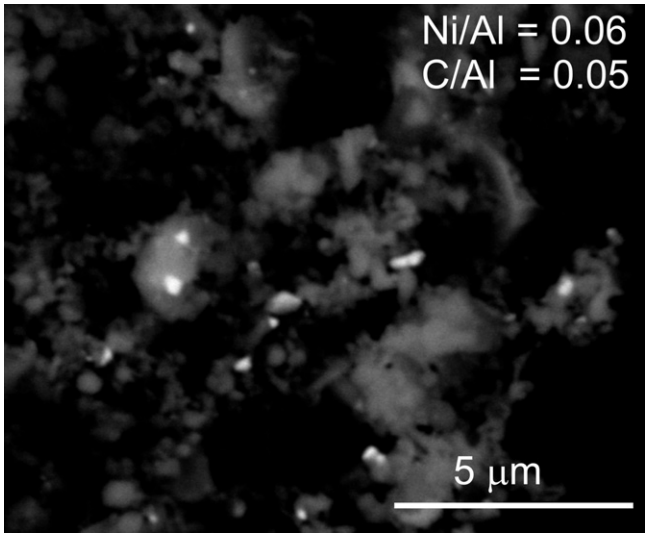

Fig. 13. Back scattered SEM image of the spent 5% Ni/Al_2O_3 catalyst: bright Ni^0 particles on the surface are visible.

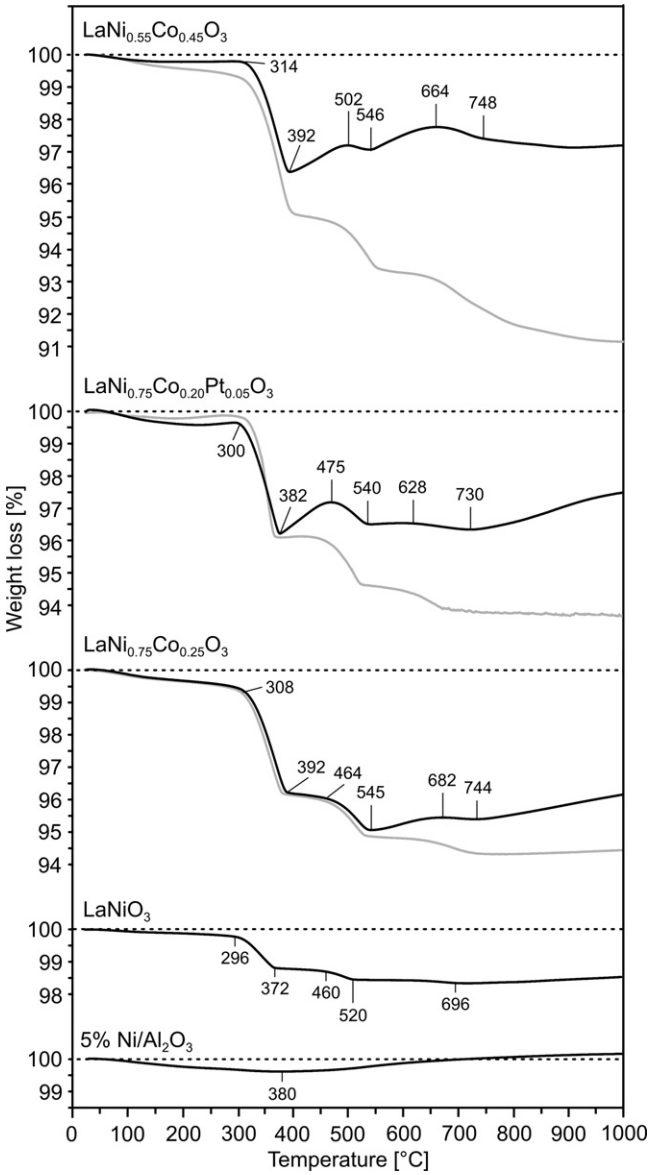

Fig. 14. TGA analysis: percent weight loss profiles of various spent catalysts performed in air (black curves) or in argon (gray curves).

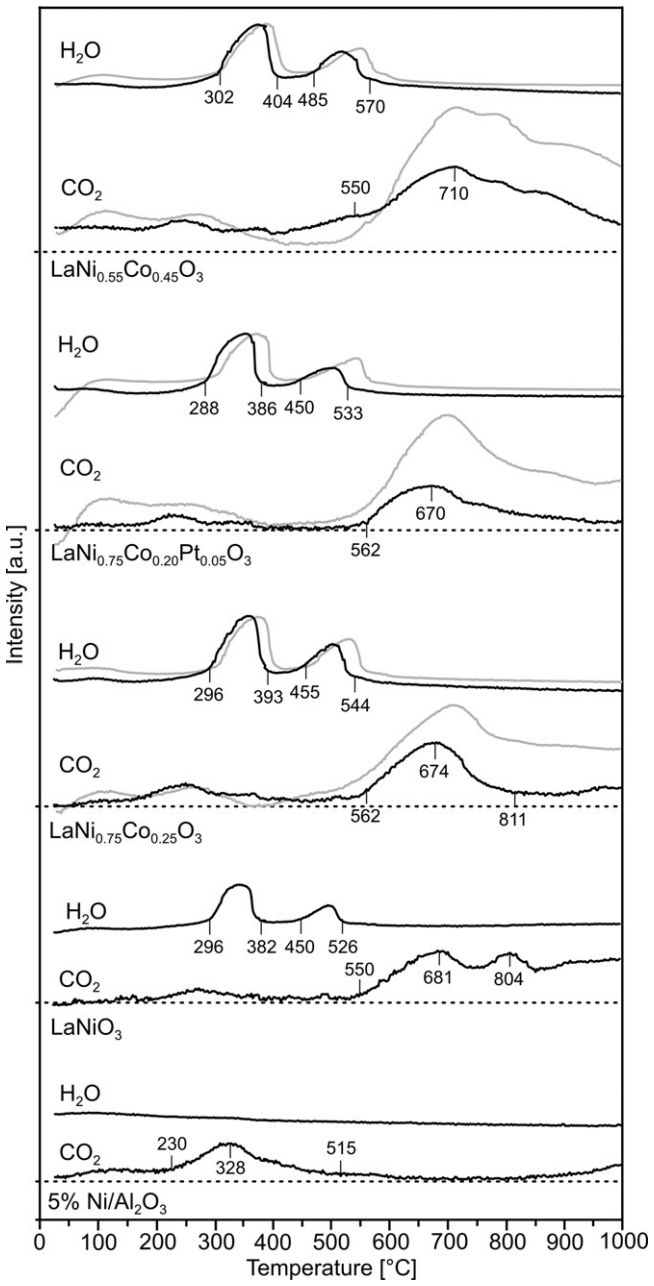

Fig. 15. H_2O and CO_2 emissions spectra from the mass spectrometer analyses associated with the TGA profiles (Fig. 14) of various spent catalysts performed in air (black curves) or in argon (gray curves).

The spent 5% Ni/Al_2O_3 showed a very limited region of mass loss, linked with a slight CO_2 emission, which ended at 380 °C, and a following region of mass increase. No release of water was detected. The mass decrease could be possibly associated with the catalytic combustion of carbonaceous residues on the catalyst surface. The catalytic combustion of coke, in fact, was evidenced at such low temperature also by other authors for Pt, Pt–Sn and Pt–Re on Al_2O_3 catalysts in the temperature range 280–420 °C [64,65]. The mass increase at high temperature could be associated with the formation of NiO, which was detected by XRD analysis.

The spent perovskite samples presented very similar trends among them. During the TGA in air, two regions of mass loss at low temperature, linked with water release, were observed, the first between approx. 290 and 390 °C and the second between 450 and 545 °C: such a double water release was fully compatible with the decomposition of the hydroxide $La(OH)_3$, detected by XRD on all the spent perovskite samples (see Fig. 12), which could be formed during the CPO reaction due to the presence of steam (side reaction) in the product gases [14]. This was in close agreement with the TGA results obtained on $LaNiO_3$ perovskite by Aman et al. [54].

For the $LaNi_{0.75}Co_{0.20}Pt_{0.05}O_3$ and $LaNi_{0.55}Co_{0.45}O_3$ perovskites, the region between the two losses of water was characterized by a marked increase of weight (not presented during the TGA in argon), linked with an exothermic effect, which could belong to the formation of NiO [54]. At temperature higher than approx. 545 °C, $LaNiO_3$ maintained an almost constant weight, whereas all the substituted perovskites showed a definite increase of weight and a marked release of CO_2, noticeable for $LaNiO_3$ too (see black curves in Figs. 14 and 15). The TGA curves obtained in argon for the substituted perovskites appeared almost overlapped up to around 545 °C. Instead at higher temperature they presented a clearly visible weight decrease, always linked with CO_2 release (see gray curves in Figs. 14 and 15). The latter was assigned to the decomposition of $La_2O_2CO_3$ phase (whose peaks were detected by XRD analysis, see Fig. 12) with subsequent mass loss [55,61]. The recorded CO_2 peaks temperatures (between 680 and 716 °C) were quite similar to that (727 °C) reported by Shirsat et al. [66] in the thermodynamic study of the decomposition of $La_2O_2CO_3$ in La_2O_3 and CO_2. Consequently, the mass increase noticed at temperatures higher than 545 °C for the substituted perovskites during the TGA in air could be associated with the formation of Co oxides (the weight increase, in fact, was more evident for the $LaNi_{0.55}Co_{0.45}O_3$ perovskite, whose presented the highest Co load), confirmed by the presence of CoO peaks on the XRD spectrum in Fig. 12. Moreover, the TGA results were in full agreements with those obtained by Villoria et al. [55] for the $LaCoO_3$ perovskite and by Sierra Gallego et al. [40,43,61] for the perovskites $LaNiO_3$, $La_{1-x}A_xNiO_{3-\delta}$ (A = Pr, Ce) and $LaNi_{1-y}B_yO_{3-\delta}$ (B = Mg, Co). The assignment of the CO_2 peaks to the decomposition of the lanthanum oxy-carbonate suggested that coke deposition over the perovskite catalysts after one test run in the CPO reactor (approx. 8 h on-stream) was very limited, in agreement with the SEM-EDX analyses. Very similar results were obtained also by Sierra Gallego et al. [61].

4. Discussion

The presence of the spinel $NiAl_2O_4$ in the fresh 5% Ni/Al_2O_3 sample, so as of NiO and Ni^0 on α-Al_2O_3 on the spent catalyst, was fully in agreement with the study performed by Dissanayake et al. [16]: employing a Ni/Al_2O_3 catalyst for the methane CPO reaction in a fixed bed, fed with a molar O_2/CH_4 ratio equal to that used in our experiments, they suggested the presence in the fixed bed of three different regions. In the inlet region, the first one encountered by the CH_4 and O_2 mixture, they detected the presence of the spinel $NiAl_2O_4$, which had only moderate activity towards CH_4 complete oxidation to CO_2 and H_2O. In a second intermediate fixed bed region, where the temperature further increased, the partial decrease in O_2 concentration (produced by the CH_4 oxidation reactions) allowed a portion of the $NiAl_2O_4$ undergoing thermal decomposition, generating α-Al_2O_3 plus a NiO surface phase, which presented an activity much higher than that of the spinel for CH_4 conversion to CO_2 and H_2O. Consequently, the complete consumption of O_2 occurred over NiO in a highly exothermic combustion process, further increasing the reactor temperature. The resulting $CH_4/CO_2/H_2O$ mixture quickly reduced NiO to Ni^0 in the remaining third region of the catalytic fixed bed. The so formed Ni^0 catalyzed the endothermic reforming reactions of the remaining CH_4 with the CO_2 and H_2O.

The stable performance of 5% Ni/Al_2O_3 indicated that, despite the dramatic SSA reduction, the active nickel on the Al_2O_3 carrier available for the reactive gases remained in a satisfactory amount for all the test time. So the catalyst did not suffer radical decrease in performance, as happened for the perovskite catalysts. After the CPO reaction, a large Ni fraction migrated to inside the particle (as confirmed by the increase of Ni/Al subsurface atomic ratio and decrease of the Ni/Al surface atomic ratio), but, anyway, a sufficient part of it remained exposed to the surface, as also visible from the SEM inspections (see Fig. 13). Thus, the high performance and stability of 5% Ni/Al_2O_3 catalyst, was only partly related to the initial high SSA, but mainly linked to Ni interactions with the high refractory alumina carrier where the active nickel species remained thermally protected in a partially embedded status, anyway easy accessible and available to the reacting gases.

On the contrary, the unsatisfactory performance of all the perovskite-based catalysts was the consequence of their high sensitivity to reduction environment. They were, in fact, exposed at very high temperatures (up to around 1200 °C) to the reducing conditions of the CPO process, where the presence of H_2O and CO_2 formed undesired phases, such $La(OH)_3$, $LaNiO_4$, NiO and $La_2O_2CO_3$, as evidenced by XRD and TGA analysis, that compromised the initial catalysts performance [7]. Compared to the fresh perovskites, the new formed Ni species were characterized by poor activity towards methane oxidation, and thus not able to maintain combustion in the first part of the catalyst bed, especially when increasing WHSV, as evidenced by the sharp decrease of T_{in}, thus moving the reforming reactions out of the catalyst zone and causing the collapse of the global reactor performance. Furthermore, the formation of $La_2O_2CO_3$ and $La(OH)_3$ over the catalyst probably created a somehow fouling layer hindering the accessibility of reagents to the Ni species active towards CPO reactions. Moreover, very recently Silva et al. [14] noticed that after reduction treatment Ni–Co perovskites completely decomposed into Co^0, Ni^0 and La_2O_3, with a decrease in the catalytic activity for PO reaction at high temperature.

5. Conclusions

The present work investigated the performance towards syngas production in a SCT-CPO reactor of five perovskite-based nickel–lanthanum catalysts ($LaNiO_3$ with Ni partially substituted with Co and Pt) and 5% Ni/Al_2O_3 supported catalyst, by varying WHSV from 130 to 560 $N l h^{-1} g_{cat}^{-1}$. Perovskite-based catalysts showed very low performances, due to the highly reducibility of the perovskite structures into La_2O_3, metallic Ni, and Ni and Co oxides and the formation of not active species, like $La(OH)_3$, La_2NiO_4 and $La_2O_2CO_3$.

On the contrary, 5% Ni/Al_2O_3 catalyst presented a very good CH_4 conversion always above 86%, which remained stable by varying WHSV. The same behaviour was noticed for H_2 and CO selectivity values, both around 90%. Furthermore, T_{in} and T_{out} values of 5% Ni/Al_2O_3 catalyst resulted quite stable by varying WHSV, whereas the perovskite-based catalysts showed a steep decrease of T_{in} and an increase of T_{out} with WHSV.

The satisfactory performance and high thermal stability of 5% Ni/Al_2O_3 catalyst, despite the relevant decrease at the end of the test runs of the BET SSA. value compared to that in the fresh status (mainly due to the alumina phase transformation from γ to α phase) and the lower Ni load compared to the subsurface Ni in the perovskite, was most likely related to nickel bonds with the Al_2O_3 support, where the active nickel particles were thermally protected as partially embedded in the carrier.

References

[1] J.N. Armor, Appl. Catal. A: Gen. 176 (1999) 159.
[2] L. Carrette, K.A. Friedrich, U. Stimming, Fuel Cells 1 (2001) 5.
[3] R. Schwiedernoch, S. Tischer, C. Correa, O. Deutschmann, Chem. Eng. Sci. 58 (2003) 633.
[4] V.R. Choudhary, A.M. Rajput, V.H. Rane, Catal. Lett. 16 (1992) 269.
[5] V.R. Choudhary, V.H. Rane, A.M. Rajput, Appl. Catal. A: Gen. 162 (1997) 235.
[6] B.C. Enger, R. Lødeng, A. Holmen, Appl. Catal. A: Gen. 346 (2008) 1.
[7] J.R. Mawdsley, T.R. Krause, Appl. Catal. A: Gen. 334 (2008) 311.
[8] Y. Wang, W. Wang, X. Hong, Y. Li, Z. Zhang, Int. J. Hydrogen Energy 34 (2009) 2252.
[9] H.W. Kim, K.M. Kang, H.-Y. Kwak, Int. J. Hydrogen Energy 34 (2009) 3351.
[10] H. Özdemir, M.A.F. Öksüzömer, M.A. Gürkaynak, Int. J. Hydrogen Energy 35 (2010) 12147.
[11] A.C. Ferreira, A.M. Ferraria, A.M. Botelho do Rego, A.P. Gonçalves, A.V. Girão, R. Correia, T.A. Gasche, J.B. Branco, J. Mol. Catal. A: Chem. 320 (2010) 47.
[12] J. Zhang, N. Zhao, W. Wei, Y. Sun, Int. J. Hydrogen Energy 35 (2010) 11776.
[13] G.G. Lenzi, E.K. Lenzi, C.V.B. Fávero, M.K. Lenzi, R.M.M. Jorge, O.A.A. dos Santos, L.M.M. Jorge, Int. J. Chem. Reactor Eng. 8 (2010) A35.
[14] C.R.B. Silva, L. da Conceição, N.F.P. Ribeiro, M.M.V.M. Souza, Catal. Commun. 12 (2011) 665.
[15] A.T. Ashcroft, P.D.F. Vernon, M.L.H. Green, Nature 344 (1990) 319.
[16] D. Dissanayake, M.P. Rosynek, K.C. Kharas, J.H. Lunsford, J. Catal. 132 (1991) 117.
[17] S. Naito, H. Tanaka, S. Kado, T. Miyao, S. Naito, K. Okumura, K. Kunimori, K. Tomishige, J. Catal. 259 (2008) 138.
[18] F.A. Silva, J.A.C. Ruiz, K.R. de Souza, J.M.C. Bueno, L.V. Mattos, F.B. Noronha, C.E. Hori, Appl. Catal. A: Gen. 364 (2009) 122.
[19] H. Tanaka, R. Kaino, Y.N.K. Tomishige, Appl. Catal. A: Gen. 378 (2010) 187.
[20] D.A. Hickman, L.D. Schmidt, Science 259 (1993) 343.
[21] L.D. Schmidt, M. Huff, Catal. Today 21 (1994) 443.
[22] R. Horn, K.A. Williams, N.J. Degenstein, A. Bitsch-Larsen, D. Dalle Nogare, S.A. Tupy, L.D. Schmidt, J. Catal. 249 (2007) 380.
[23] A.S. Bodke, S.S. Bharadwaj, L.D. Schmidt, E. Ranzi, Science 285 (1999) 712.
[24] O. Deutschmann, L.D. Schmidt, AIChE J. 44 (1999) 2465.
[25] D.K. Zerkle, M.D. Allendorf, M. Wolf, O. Deutschmann, J. Catal. 196 (2000) 18.
[26] L. Basini, K. Aasberg-Petersen, A. Guarinoni, M. Ostberg, Catal. Today 64 (2001) 9.
[27] K.L. Hohn, L.D. Schmidt, Appl. Catal. A: Gen. 211 (2001) 53.
[28] M. Prettre, Ch. Eichner, M. Perrin, Trans. Faraday Soc. 42 (1946) 335.
[29] W.J.M. Vermeiren, E. Blomsma, P.A. Jacobs, Catal. Today 13 (1992) 427.
[30] Q.G. Yan, T.H. Wub, W.Z. Weng, H. Toghiani, R.K. Toghiani, H.L. Wan, C.U. Pittman Jr., J. Catal. 226 (2004) 247.
[31] Platinum Today, Johnson Matthey, London, September 2010, www.platinum.matthey.com.
[32] S. Wang, G.Q. Lu, Appl. Catal. A: Gen. 169 (1998) 271.
[33] Y. Zhang, G. Xiong, S. Sheng, W. Yang, Catal. Today 63 (2000) 517.
[34] T. Utaka, S.A. Al-Drees, J. Ueda, Y. Iwasa, T. Takeguchi, R. Kikuchi, K. Eguchi, Appl. Catal. A: Gen. 247 (2003) 125.
[35] J. Requies, M.A. Cabrero, V.L. Barrio, M.B. Güemez, J.F. Cambra, P.L. Arias, F.J. Pérez-Alonso, M. Ojeda, M.A. Peña, J.L.G. Fierro, Appl. Catal. A: Gen. 289 (2005) 214.
[36] L. De Rogatis, T. Montini, A. Cognigni, L. Olivi, P. Fornasiero, Catal. Today 145 (2009) 176.
[37] C. Batiot-Dupeyrat, G. Valderrama, A. Meneses, F. Martinez, J. Barrault, J.M. Tatibouët, Appl. Catal. A: Gen. 248 (2003) 143.
[38] C. Batiot-Dupeyrat, G.A. Sierra Gallego, F. Mondragón, J. Barrault, J.-M. Tatibouët, Catal. Today 107–108 (2005) 474.
[39] S.M. Lima, J.M. Assaf, M.A. Peña, J.L.G. Fierro, Appl. Catal. A: Gen. 311 (2006) 94.
[40] G.A. Sierra Gallego, F. Mondragón, J. Barrault, J.-M. Tatibouët, C. Batiot-Dupeyrat, Appl. Catal. A: Gen. 311 (2006) 164.
[41] M.E. Rivas, J.L.G. Fierro, M.R. Goldwasser, E. Pietri, M.J. Pérez-Zurita, A. Griboval-Constant, G. Leclercq, Appl. Catal. A: Gen. 344 (2008) 10.
[42] G.C. de Araujo, S.M. de Lima, J.M. Assaf, M.A. Peña, J.L.G. Fierro, M.C. Rangel, Catal. Today 133–135 (2008) 129.
[43] G.A. Sierra Gallego, C. Batiot-Dupeyrat, J. Barrault, E. Florez, F. Mondragón, Appl. Catal. A: Gen. 334 (2008) 251.
[44] S.M. de Lima, A.M. da Silva, L.O.O. da Costa, J.M. Assaf, G. Jacobs, B.H. Davis, L.V. Mattos, F.B. Noronha, Appl. Catal. A: Gen. 377 (2010) 181.
[45] G.C. de Araujo, S. Lima, M.C. Rangel, V. La Parola, M.A. Peña, J.L.G. Fierro, Catal. Today 107–108 (2005) 906.
[46] J.A. Villoria, M.C. Alvarez-Galvan, R.M. Navarro, Y. Briceño, F. Gordillo Alvarez, F. Rosa, J.L.G. Fierro, Catal. Today 138 (2008) 135.
[47] L.D. Vella, S. Specchia, Catal. Today, in press.
[48] C.D. Wagner, L.E. Davis, M.V. Zeller, J.A. Taylor, R.H. Raymond, L.H. Gale, Surf. Interface Anal. 3 (1981) 211.
[49] S. Specchia, G. Negro, G. Saracco, V. Specchia, Appl. Catal. B: Environ. 70 (2007) 525.
[50] S. Specchia, L.D. Vella, B. Lorenzut, T. Montini, V. Specchia, P. Fornasiero, Ind. Eng. Chem. Res. 49 (2010) 1010.
[51] M.N. Natile, E. Ugel, C. Maccato, A. Glisenti, Appl. Catal. B: Environ. 72 (2007) 351.
[52] B.W. Hoffer, A.D. van Langeveld, J.P. Janssens, R.L.C. Bonné, C.M. Lok, J.A. Moulijn, J. Catal. 192 (2003) 432.
[53] M. Biswas, J. Alloys Compd. 480 (2009) 942.
[54] D. Aman, T. Zaki, S. Mikhail, S.A. Selim, Catal. Today 164 (2011) 209.

[55] J.A. Villoria, M.C. Alvarez-Galvan, S.M. Al-Zahrani, P. Palmisano, S. Specchia, V. Specchia, J.L.G. Fierro, R.M. Navarro, Appl. Catal. B: Environ., in press, doi:10.1016/j.apcatb.2011.04.010.
[56] S. Bernal, F.J. Botana, R. García, J.M. Rodríguez-Izquierdo, React. Solids 4 (1987) 23.
[57] K. Tomishige, S. Kanazawa, K. Suzuki, M. Asadullah, M. Sato, K. Ikushima, K. Kunimori, Appl. Catal. A: Gen. 233 (2002) 35.
[58] L.D. Vella, T. Montini, S. Specchia, P. Fornasiero, Int. J. Hydrogen Energy, in press.
[59] L. De Rogatis, M. Cargnello, V. Gombac, B. Lorenzut, T. Montini, P. Fornasiero, Chem. Sus. Chem. 3 (2010) 24.
[60] K. Traina, M.C. Steil, J.P. Pirard, C. Henrist, A. Rulmont, R. Cloots, B. Vertruyen, J. Eur. Ceram. Soc. 27 (2007) 3469.
[61] G.A. Sierra Gallego, J. Gallego Marín, C. Batiot-Dupeyrat, J. Barrault, F. Mondragón, Appl. Catal. A: Gen. 369 (2009) 97.
[62] A. Beretta, P. Forzatti, J. Catal. 200 (2001) 45.
[63] I. Tavazzi, A. Beretta, G. Groppi, M. Maestri, E. Tronconi, P. Forzatti, Catal. Today 129 (2007) 372.
[64] C.L. Pieck, E.L. Jablonski, J.M. Parera, Appl. Catal. 70 (1991) 19.
[65] C.L. Pieck, C.R. Vera, C.A. Querini, J.M. Parera, Appl. Catal. A: Gen. 278 (2005) 173.
[66] A.N. Shirsat, M. Ali, K.N.G. Kaimal, S.R. Bharadwaj, D. Das, Thermochim. Acta 399 (2003) 167.